THE JOURNAL OF BIOLOGICAL CHEMISTRY
Vol. 278, No. 28, Issue of July 11, pp. 25910–25918, 2003
Printed in U.S.A.

Structural and Folding Dynamic Properties of the T70N Variant of Human Lysozyme*[S]

Received for publication, October 28, 2002, and in revised form, April 22, 2003
Published, JBC Papers in Press, April 22, 2003, DOI 10.1074/jbc.M211000200

Gennaro Esposito‡, Julian Garcia‡§, Palma Mangione¶, Sofia Giorgetti¶, Alessandra Corazza‡, Paolo Viglino‡, Fabrizio Chiti‖, Alessia Andreola¶, Pascal Dumy§, David Booth, Philip N. Hawkins**, and Vittorio Bellotti¶‡‡**

*From the ‡Dipartimento di Scienze e Tecnologie Biomediche, Università di Udine, 33100 Udine, Italy, the §Laboratoire d'Etudes Dynamiques et Structurales de la Séléctivité, University Joseph Fourier of Grenoble, 38041 Grenoble Cedex 9, France, the ¶Dipartimento di Biochimica, Università di Pavia, Centro Interdipartimentale di Biologia Applicata, Laboratorio Biotecnologie Istituto di Ricovero e Cura a Carattere Scientifico, Policlinico San Matteo Pavia, 27100 Pavia, Italy, the ‖Dipartimento di Science Biochimiche, Università di Firenze, 55100 Firenze, Italy, and the **Centre for Amyloidosis and Acute Phase Proteins, Department of Medicine, Royal Free and University College Medical School, London NW3 2PF, United Kingdom*

Definition of the transition mechanism from the native globular protein into fibrillar polymer was greatly improved by the biochemical and biophysical studies carried out on the two amyloidogenic variants of human lysozyme, I56T and D67H. Here we report thermodynamic and kinetic data on folding as well as structural features of a naturally occurring variant of human lysozyme, T70N, which is present in the British population at an allele frequency of 5% and, according to clinical and histopathological data, is not amyloidogenic. This variant is less stable than the wild-type protein by 3.7 kcal/mol, but more stable than the pathological, amyloidogenic variants. Unfolding kinetics in guanidine are six times faster than in the wild-type, but three and twenty times slower than in the amyloidogenic variants. Enzyme catalytic parameters, such as maximal velocity and affinity, are reduced in comparison to the wild-type. The solution structure, determined by ^{1}H NMR and modeling calculations, exhibits a more compact arrangement at the interface between the β-sheet domain and the subsequent loop on one side and part of the α domain on the other side, compared with the wild-type protein. This is the opposite of the conformational variation shown by the amyloidogenic variant D67H, but it accounts for the reduced stability and catalytic performance of T70N.

Amyloidosis is an emerging category of diseases characterized by the extracellular accumulation of protein aggregates that share a common fibrillar conformation. The 20 proteins that can generate amyloid deposits in humans are extremely heterogeneous in function and structure, but, along the pathological transformation leading to aggregation and precipitation, all of them exhibit the same peculiar conformational pattern named cross-β structure, irrespective of the parent-starting arrangement (1). The lack of any sequence similarity and folding analogy among the amyloid-forming proteins led Dobson to conclude that the ability to form cross-β structure, wherein hydrogen bonds are formed between polypeptide chains in directions parallel to the fiber axis, is a generic property of polypeptide chains (2). Investigations of structure (3–4), folding dynamics (5–7), and fibrillogenesis (3, 8) of the initially reported amyloidogenic variants of lysozyme have made important contributions to a better understanding of the process involved in the conversion of globular proteins into amyloid fibrils. Amyloidogenic lysozyme represents probably the most convenient and informative model of fibrillogenesis from a globular protein. Besides being, in fact, one of the best characterized enzymes, its fibrillogenic mechanism is not influenced by protein fragmentation; nor, to our knowledge, does the wild-type species generate amyloid deposits *in vivo*, even in the elderly. Thorough analysis of several biochemical properties of the amyloidogenic variants in comparison to the wild-type species showed that pathogenic lysozymes are less stable than wild-type (3–8). This thermodynamic destabilization correlates with an increased concentration of partly unfolded intermediates that self-aggregate into fibrillar polymers. In this study we present the biochemical and structural characterization of a new natural variant of human lysozyme, T70N (9), that displays the general properties of a less stable and less efficient enzyme in comparison to wild-type but does not undergo pathological fibrillar conversion *in vivo*. The T70N variant is present in the British population with an allele frequency of 5% (9). The comparison of the biochemical characteristics of this variant with those of the amyloidogenic species can highlight the role of some of the folding abnormalities identified in the pathogenic species.

EXPERIMENTAL PROCEDURES

Clinical Studies—Genotyping for lysozyme T70N was performed as described previously (9) in 110 patients with systemic amyloidosis referred to the United Kingdom Centre for Amyloidosis, whose amyloid fibril type was initially uncharacterized but in whom the clinical phe-

* The work of the Centre for Amyloidosis and Acute Phase Proteins is supported by grants from Medical Research Council, the Wellcome Trust, the Wolfson Foundation and National Health Service Research and Development Funds. The National Health Service National Amyloidosis Centre is funded by the United Kingdom Department of Health. This work was also supported by the financial contribution of "Ministero della Sanità Italia" (Ricerca finalizzata sulla malattia di Alzheimer, 020ALZ00/01), DSTB, Telethon (grant number GP0186Y/01), "Ministero della Università e Ricerca Scientifica Italy (through Fondo per gli Investimenti della Ricerca di Base 2002-2005 and COFIN 2002058218_003 projects) and by Fondazione CARIPLO. The costs of publication of this article were defrayed in part by the payment of page charges. This article must therefore be hereby marked "*advertisement*" in accordance with 18 U.S.C. Section 1734 solely to indicate this fact.

[S] The on-line version of this article (available at http://www.jbc.org) contains Table S1 (^{1}H chemical shifts and amide protection factors), Table S2 (NOE restraint list from NMR data of T70N lysozyme), Fig. S1 (distance restraint histograms), Fig. S2 (TOCSY and NOESY fingerprints), and Fig. S3 (overview contour maps).

‡‡ To whom correspondence should be addressed: Dipartimento di Biochimica-Università di Pavia, Via Taramelli 3/b, 27100 Pavia, Italy. Tel.: 39-0382-507783; Fax: 39-0382-423108; E-mail: vbellot@unipv.it.

notype was consistent with lysozyme amyloidosis. The variant was also sought in 23 patients with amyloid A amyloidosis and complicating rheumatoid arthritis and 60 patients with immunoglobulin light chain (AL)[1] amyloidosis.

Protein Expression—Mutagenesis, expression, and purification of human lysozymes were performed as described previously (3).

Equilibrium Denaturation—Guanidine hydrochloride (GdnHCl)-induced unfolding of lysozymes was monitored by intrinsic fluorescence emission at 340 nm with excitation of 295 nm. Fluorescence measurements were performed on a PerkinElmer LS50 spectrofluorometer at 20 °C using a 10-mm light path cell. The protein solution (0.01 mg/ml) was incubated for 1 h at increasing concentrations of GdnHCl in sodium phosphate buffer, pH 6.5. The change of fluorescence as a function of denaturant concentration was analyzed according to the method described by Santoro and Bolen (10) to determine the main thermodynamic parameters of the unfolding reaction.

Thermal Unfolding—Far and near UV circular dichroism (CD) spectra were recorded on a JASCO 710 spectropolarimeter equipped with a temperature control system using 1- and 10-mm path length quartz cuvettes over the wavelength ranges 200–240 nm and 250–310 nm, respectively. The protein concentration was 200 μg ml^{-1} in H_20, pH 5, and the CD data were expressed as mean residue ellipticity (θ). The measurements were collected at different constant temperatures from 20 to 90 °C. Equilibrium thermal unfolding of T70N lysozyme was monitored by ellipticity values at 222 and 270 nm and then normalized to the fraction of unfolded protein using $f_u = (\theta-\theta_N)/(\theta_U-\theta_N)$, where θ is the observed parameter and θ_N and θ_U are the ellipticities of the native and unfolded protein, respectively, extrapolated from the pre- and post-transition baselines at the corresponding temperatures.

Enzyme Kinetics and Inhibitor Affinity—Lysozyme enzyme kinetics were determined with *p*-nitrophenol penta-*N*-acetyl-β-chitopentaoside (PNP-$(GlcNAc)_5$) (11). Reaction mixtures (1 ml) containing 10 μg of each type of lysozyme, 0.1 unit of β-*N*-acetyl-hexosaminidase (NAHase), and various concentrations of PNP-$(GlcNAc)_5$ (from 6 to 60 μM) in 0.1 M citrate buffer, pH 5.0, were incubated at 37 °C. The enzymatic reaction was stopped after 25 min by adding 2 M Na_2CO_3 (0.5 ml), and then the resulting free *p*-nitrophenol was determined spectrophotometrically at 405 nm. Affinity to the chitotriose $(NAG)_3$ was estimated by fluorescence measurements (12) on a PerkinElmer LS50 spectrofluorometer at 30 °C in MacIlvaine's buffer (100 mM citric acid and 50 mM Na_2HPO_4, pH 7.2). Protein concentration was adjusted to 3 μM. Excitation and emission wavelengths were 285 and 325 nm, respectively. Affinity constants were determined by plotting log $(F_o - F)/(F - F_\infty)$ against log [S], where F_o, F, and F_∞ are the fluorescence intensities of solutions of enzyme alone, enzyme in the presence of a concentration [S] of $(NAG)_3$, and enzyme saturated with the inhibitor, respectively.

Unfolding-Refolding Kinetics—Unfolding and refolding experiments were carried out with a Bio-Logic SFM3 stopped flow fluorometer by using an excitation wavelength of 285 nm and monitoring the total fluorescence emission change over 320 nm. All of the experiments were performed at 20 °C with a cell path length of 2.0 mm. For unfolding experiments, 1 volume of each type of protein in 20 mM acetate at pH 5.0 was 10-fold diluted with a solution containing 6 M GdnHCl at pH 5.0. The refolding reactions were carried out by mixing 1 volume of enzyme in 6 M GdnHCl with 10 volumes of 20 mM acetate at pH 5.0.

NMR Spectroscopy and Modeling—NMR spectra were obtained at 500.13 MHz and 37 °C with a Bruker Avance spectrometer on 0.7–0.8 mM protein samples dissolved in H_2O/D_2O (95:5) or 99.9% D_2O. No addition was done to adjust the uncorrected pH meter reading that was 4.2 for all measurements except for the isotope exchange and the conformational analysis experiments, where the values ranged between 4.5 and 4.9. A number of two-dimensional TOCSY (13), DQF-COSY (14), and NOESY (15) spectra were acquired with the sculpting scheme for solvent suppression (16) using selective pulses of 3–5 ms, 1.1 s steady state recovery time, mixing times (t_m) of 20–50 ms for TOCSY and 100 ms for NOESY, t_1 quadrature detection by TPPI (17), or States method (18) or gradient-assisted coherence selection (echo/anti-echo) (19). The spin-lock mixing of the TOCSY experiment was obtained with MLEV17 (20) or DIPSI-2 (21) pulse trains at $\gamma B_2/2\pi$ = 9–10 kHz. The acquisitions were performed over a spectral width of 7002.8 Hz in both dimensions, with matrix size of 1024–2048 points in t_2 and 256–512 points in t_1 and 32–128 scans/t_1 free induction decay (FID). Selective one-dimensional NOESY experiments for temperature coefficient measurements were run by replacing the first two 90° pulses of the standard sequence with selective Gaussian-shaped pulses of 6 ms centered on the side-chain amide resonance of interest. The water resonance was suppressed by appending an excitation-sculpting module (16) to the non-selective detection pulse. The acquisitions were performed between 33 and 40 °C by collecting 512 scans over 2^{13} data points to monitor the chemical shift of the exchanging, unperturbed side-chain-amide resonance with sufficient precision ($\Delta\delta = \pm$ 0.8 ppb). Isotope exchange data were collected in either forward (D_2O) and backward mode (H_2O) by consecutive acquisition of TOCSY spectra (2.5 h/spectrum in D_2O and 15 min/spectrum in H_2O) over variable time intervals from solvent addition (6, 12, or 24 h). For the fast acquisitions in H_2O, only 80 t_1 increments were collected, and the standard linear prediction routine of Bruker software was employed to expand the indirect dimension to 200 data points with 40 coefficients prior to two-dimensional Fourier transform. Protection factors were obtained from the ratio between intrinsic (calculated) and apparent (experimental) isotope exchange rates. The intrinsic rates were computed through the parameters and procedures reported by Bai *et al.* (22). All spectra were referenced on the I106 $C^{\gamma}H_3$ resonance at −0.61 ppm as reported previously (23). Data processing and analysis were performed using Felix (Accelrys, San Diego, CA) software with shifted (60–90°) square sinebell apodization and polynomial baseline correction for NOESY data. Internuclear distances were quantified from the cross-peak volumes of the NOESY spectra using some cross-peaks from Trp-64 as calibrants. Tethered molecular dynamic (MD) simulations were performed by using the Discover software (Accelrys), following the default protocol for simulated annealing starting at a temperature of 600 K slowly lowered to 300 K (time step = 1 fs, 8.6 ps MD, 500 conjugate-gradient minimization steps) (24). The selected force field was AMBER, and, to shorten the range of Coulomb interaction, a distance-dependent relative dielectric constant, ϵ_r, was used ($\epsilon_r(r) = 4r$). Molecular structures were generated with Insight II (Accelrys). To assess and improve the accuracy of the NOE restraint set, the theoretical NOESY spectrum was back-calculated using the matrix doubling module of Felix (total correlation time, 2 ns) and compared with the experimental one. The restraints were subsequently refined, and a new MD was performed until good concordance was reached between theoretical and experimental NOESY spectra.

RESULTS

T70N Lysozyme Is Not Amyloidogenic in Vivo—Several clinical and biochemical findings suggest that T70N lysozyme is not amyloidogenic. The allele frequency of T70N is relatively high in the normal population (5/100) (9). Both I56T and D67H are very rare and have only been identified in kindreds with amyloidosis wherein there is 100% penetrance (25). If T70N was as amyloidogenic as these variants, 5% of the British population might be expected to have amyloidosis. However, no individual with T70N lysozyme amyloidosis has ever been identified. This has been the case despite investigations designed to identify such individuals. Amyloid fibril type is ultimately identified in all patients presenting at the United Kingdom Centre for Amyloidosis. Prior to fibril identification, the prevalence of the T70N lysozyme allele was determined in patients with systemic amyloidosis, the clinical phenotype associated with I56T and D67H lysozyme amyloidosis. In these 55 patients, the T70N allele frequency was 0.08 (9/110 alleles, including one homozygote), similar to the allele frequency in the normal population. In all other patients with amyloidosis seen at the clinic, the fibril type had been characterized (except one, see below). In these eight patients carrying at least one T70N allele, the amyloid fibril type was subsequently identified as serum amyloid A (two patients), AL amyloid (four patients), not amyloidosis (one patient, the homozygote), and hereditary amyloidosis of unknown fibril type (one patient). In the one patient with hereditary systemic amyloidosis, the fibril protein has yet to be characterized. It is not lysozyme, and an individual in the kindred has the T70N lysozyme but not amyloid. These data are consistent with the hypothesis that T70N variant does not cause systemic amyloidosis in the British population.

[1] The abbreviations used are: AL, immunoglobulin light chain amyloidosis; CD, circular dichroism; DQF-COSY, double quantum-filtered correlation spectroscopy; GdnHCl, guanidine hydrochloride; MD, molecular dynamic; $(NAG)_3$, β-1,4-linked trimer of N-acetyl-D-glucosamine; NOE, nuclear Overhauser effect; NOESY, NOE spectroscopy; TOCSY, total correlation spectroscopy.

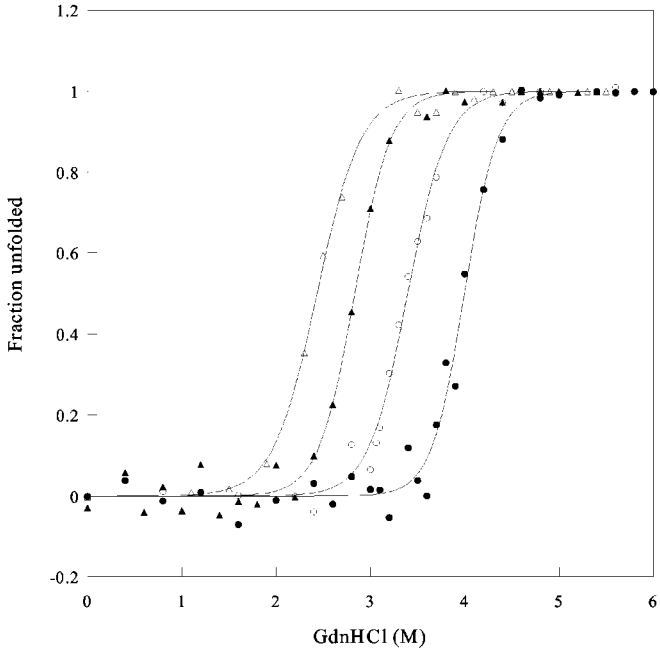

FIG. 1. **Equilibrium GdnHCl denaturation curve.** GdnHCl unfolding curves for the wild-type (●), T70N (○), D67H (▲), and I56T lysozymes (△) at pH 6.5 and 20 °C are shown. The *solid lines* represent the results of the fitting procedure.

To test whether there was co-deposition of lysozyme within the amyloid fibrils created by other proteins, we have isolated the natural amyloid fibrils from amyloid deposits of one heterozygous T70N heterozygote patient clearly affected by AL amyloidosis. No lysozyme was detected in the fibrils by immunoblot. To test whether T70N lysozyme was interacting with other fibril types, the allele frequency in rheumatoid arthritis patients (2 T70N from 56 alleles) and AL (4/120) amyloidosis groups was compared. Asn-70 was not over- or under-represented, thus neither promoting nor inhibiting fibril formation. Finally, in the one subject homozygous for the mutation, serum lysozyme concentration was determined, and, according to the lysoplate method, the circulating protein was 12 mg/liter (nv 4–13 mg/liter.)

Equilibrium Denaturation of T70N Lysozyme—The unfolding of the T70N variant was monitored at equilibrium by intrinsic fluorescence emission at 340 nm as a function of denaturant concentration at pH 6.5 and 20 °C. The unfolding curves for the wild-type, T70N, I56T, and D67H, normalized to the fraction of unfolded protein (f_u), are shown in Fig. 1. All transitions are characterized by the presence of a single sharp change in the fluorescence intensity that is typical of cooperative transition in a two-state system. The transition midpoints are reduced, as compared with that of the wild-type protein, by 0.5, 0.9, and 1.3 denaturant concentration units for the T70N, D67H, and I56T, respectively. The data for the I56T and D67H variants are in good agreement with previous data of Takano *et al.* (6). The values of ΔG^{H_2O} of unfolding, calculated according to Santoro and Bolen (10), indicate that the three variants, T70N, D67H and I56T, are destabilized, in comparison to the wild-type, by 3.7, 4.7, and 7.2 kcal/mol, respectively.

Thermal Unfolding—We have used circular dichroism to monitor T70N lysozyme unfolding behavior upon heating from 20 to 90 °C. The measurements were performed in the far and near UV regions (Fig. 2, *a* and *b*) to estimate the equilibrium thermal unfolding of the protein at pH 5. The coincidence of the two transition curves by the CD data at 222 and 270 nm, normalized to the apparent fraction of unfolded species (Fig. 2*c*), was observed over the entire temperature range studied. Such behavior is quite similar to the cooperative two-state unfolding displayed by the wild-type protein under these conditions (3), even if the midpoint of thermal denaturation of T70N variant is 3 °C below that of the wild-type lysozyme. From the analysis of CD measurements, there is no evidence of the existence of an intermediate state with a helical secondary structure but lacking tertiary interactions as was previously documented in the amyloidogenic species (3).

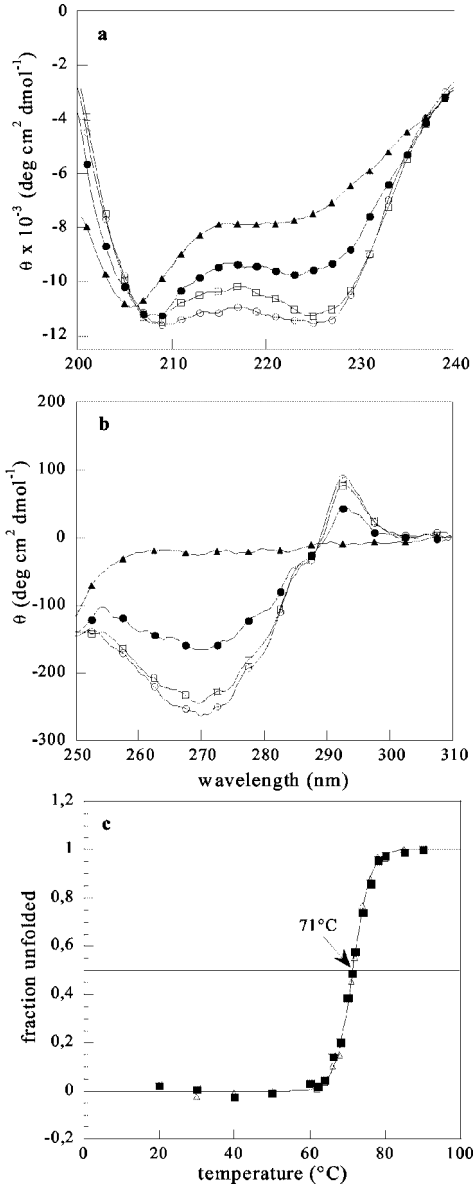

FIG. 2. **Thermal denaturation of T70N lysozyme.** CD spectra in the far UV (*a*) and near UV (*b*) of the protein in water at pH 5 and recorded at 20 (○), 60 (□), 70 (●), and 90 °C (▲) are shown. Unfolded fraction of T70N lysozyme (*c*) was estimated from the ellipticities at 222 nm (■) and 270 nm (△) as a function of temperature. The midpoint of thermal denaturation is 71 °C.

Enzyme Catalysis Performance—The enzyme kinetics data (Table I) suggest that T70N lysozyme has a reduced enzymatic activity with respect to wild-type, comparable with that reported for the D67H variant. This comparatively poor performance is the combined result of both a lower substrate affinity and a less efficient turnover. The reduced affinity of T70N for the chitotriose $(NAG)_3$, the trisaccharide inhibitor of lysozyme, which can be inferred from the dissociation constant (K_d) value of Table I, is also confirmed in D67H and I56T, but the T70N

TABLE I
Comparative summary of the biochemical properties of the wild-type and three human lysozyme variants

Protein	C_m [a]	ΔG^{H_2O} [b]	$\Delta\Delta G^{H_2O}$ [c]	K_m [d]	k_{cat} [d]	K_d [e]	k_{unf} [f]
	M	kcal·mol^{-1}	kcal·mol^{-1}	μM	M·s^{-1}	μM	s^{-1}
Wild type	4	13.7		16.5	14.5	25 ± 5	0.0157 ± 0.002
T70N	3.4	9.99	3.71	30	10	158 ± 45	0.095 ± 0.014
I56T	2.4	6.47	7.23	18.5	15	46 ± 11	0.34 ± 0.03
D67H	2.8	8.99	4.71	38	9.5	60 ± 12	2.04 ± 0.16

[a] GdnHCl concentration of the midpoint of equilibrium denaturation; experimental error is ~0.1 M.
[b] Free energy change in the absence of denaturant; experimental error is ~10%.
[c] $\Delta\Delta G^{H_2O} = \Delta G^{H_2O}$ (mutant) − ΔG^{H_2O} (wild type).
[d] Enzyme activities determined with PNP-$(GlcNAc)_5$; experimental errors are ~20% for K_m and 5% for k_{cat}.
[e] Dissociation constants for $(NAG)_3$ obtained at pH 7.2 and 30 °C; values are mean ± standard deviation.
[f] Unfolding rate constants determined at pH 5 with 5.4 M GdnHCl, and 20 °C; values are mean ± standard deviation.

variant has the lowest affinity for $(NAG)_3$ of the all natural human lysozyme variants.

Unfolding-Refolding Kinetics of Mutant Human Lysozymes—To assess the effects of the T70N substitution on the folding and unfolding kinetics, comparative stopped-flow kinetic studies of the reversible unfolding-refolding process were performed. The unfolding-refolding reactions were monitored by fluorescence intensity. The unfolding kinetics of T70N are described by a single exponential function, as reported previously (5–6). The refolding reaction from the guanidine-denatured protein consists of two phases in which the fast phase is predominant, in amplitude, over the slow phase as shown previously (5–6). No significant differences were found between T70N variant and the wild-type protein in the rates of the refolding phases (data not shown). On the contrary, the unfolding process of the T70N is 3–4 times faster than that of the wild-type protein. Fig. 3 depicts the unfolding kinetics of wild-type, T70N, D67H, and I56T. The unfolding rates for the amyloidogenic mutants are consistent with the data reported previously by Canet *et al.* (5) and Takano *et al.* (6) and are, respectively, three and twenty times faster than that of the T70N variant.

^{1}H NMR Chemical Shift Changes—Based on the assignments of wild-type human lysozyme (23) and amyloidogenic variants (4), the ^{1}H chemical shifts for all residues of the T70N lysozyme were carefully controlled (at least for the backbone resonances) by standard methodology (27). The deviations of the H^N chemical shift values with respect to the wild-type protein are shown in Fig. 4*a*. Comparison with the corresponding histograms reported for the I56T and D67H mutants (4) suggests that the T70N variant has a $\Delta\delta H^N$ pattern somehow intermediate, *i.e.* whereas the extent of δH^N deviations is generally limited, similar to I56T, a number of $\Delta\delta H^N$ above the average are observed, as with D67H, for residues 52, 63, 64, 67, 72, and 77 (upfield) and residues 68, 69, 73, 76, and 79 (downfield). The interpretation of amide chemical shift changes may be complex and tricky, but there is no doubt that all of the variations seen with T70N are spread over the corresponding locations of the β-sheet, the subsequent loop, and the following 3_{10} helix segment of the wild-type structure. For proteins, ^{1}H NMR chemical shifts exhibit an established correlation with secondary structure only for H^α resonances (28). When compared with D67H, the δH^α of T70N show meaningful differences only at positions 51, 61, 66, 68, 73, and 80 (Fig. 4*b*). In general, the accepted threshold for meaningful difference, *i.e.* $\Delta\delta H^a \cong \pm 0.1$ ppm, refers to comparison with peptides in a statistically disordered conformation. Thus, to ascertain meaningfulness, the deviations of Fig. 4*b* were analyzed against the corresponding parameters obtained from the comparison with the wild-type protein data, which, in turn, were compared with the basic peptide shifts. In particular, on moving from the D67H to the T70N mutant, the downfield shifts at residues 51, 61, and 66 suggest that the conformation and extension of the β strands of the wild-type tend to be restored. Similarly, a recovery of the wild-type geometry at the end of the turn-like segment 70–73 is likely to be responsible of the opposite shift observed for residue 73. An analogous interpretation applies also to the upfield shift of residue 68 and the downfield shift of residue 80.

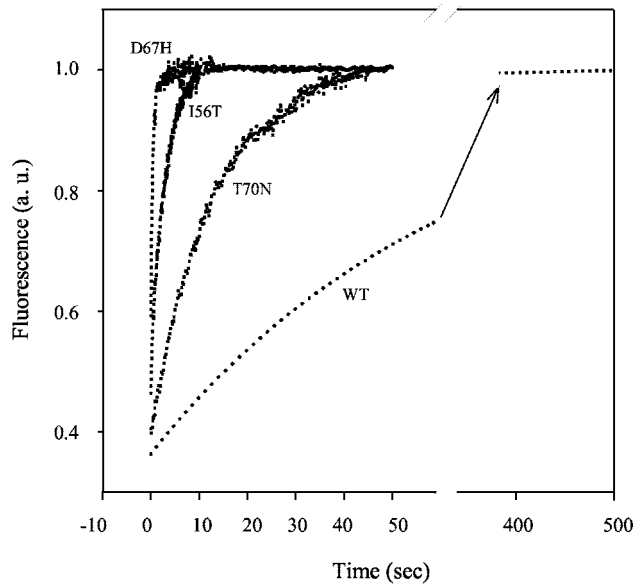

FIG. 3. **Unfolding kinetics monitored by stopped flow fluorescence.** The kinetic traces of four human lysozyme variants were acquired at pH 5 with 5.4 M GdnHCl at 20 °C. The data have been scaled to unit amplitude (*a. u.*) of the fluorescence of the unfolded species.

Restrained Modeling—To test the structural inference obtained from the assignment and analysis of chemical shift changes in mutant T70N with respect to D67H, I56T, and wild-type proteins, a number of unambiguously classified NOEs, connecting hydrogens in the region 41–92 of the investigated mutant, were quantified to extract the relative internuclear separations. The substantial invariance of the chemical shifts of T70N with respect to the wild-type protein in the fragments that flank the region 41–92 should grossly reflect a persistence of the local spatial arrangement of the canonical structure. It appears therefore conceivable to adopt the geometry of the original structure outside the fragment 41–92. To constrain part of the structure in a fixed arrangement, tethered MD simulations were performed using the standard tools of Discover software (Accelrys) (24). Because of the high degree of signal overlap in the lysozyme spectrum, the collection of the NOESY cross-peaks for quantitative purposes was necessarily limited to resolved correlations of the selected region resonances. Overall, 125 internuclear distances, mostly medium

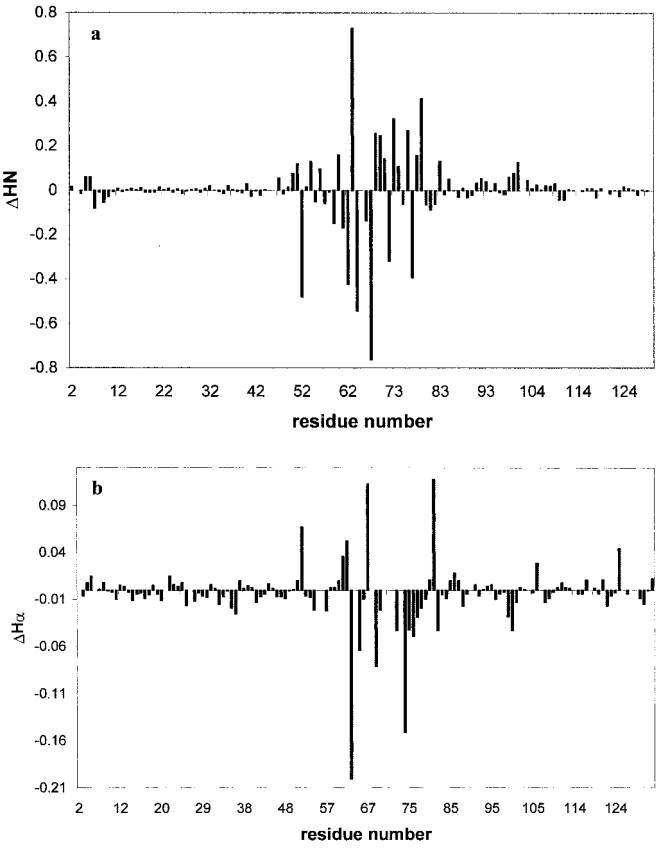

FIG. 4. **^{1}H NMR chemical shift changes.** Chemical shift changes of H^N (*a*) and H^α (*b*) resonances of T70N lysozyme with respect to the corresponding values in the wild-type (*a*) and D67H (*b*) species.

and long-range ones, were estimated and employed for the tethered MD calculations. Two simulation cycles were performed with the same set of experimental distance restraints and parameters, but with two different starting geometries in analogy to the structural deviations of the amyloidogenic lysozyme variants with respect to wild-type protein (3). The wild-type lysozyme structure, in practice the same as that of I56T mutant or the structure of D67H mutant (PDB coordinate codes 1REX and 1LYY, respectively) (3), were alternatively imposed on the T70N sequence. The starting conformations diverge only in correspondence of the β-sheet and subsequent loop (3), *i.e.* within the region 41–92 that was left untethered and restrained only by the experimental distances in MD runs. The results are displayed in Fig. 5, where the backbones of the two final and the two starting structures are superimposed in the regions of interest. It can be readily seen that both the MD-restrained structures converge toward a conformation similar to the wild-type protein, irrespective of the starting arrangement. More precisely, the calculated structures appear to adopt an even more compact arrangement than the wild-type one, because the loop 66–74 and the turn 47–50 consistently shift in the same direction toward the helical domain, just the contrary of the shifts observed in D67H. Although the tertiary structure resulting from a tethered MD simulation should be regarded with some caution when the extent of fixed and restrained molecular moieties are comparable, the outcome of the calculation is in qualitative agreement with the conclusions that were reached from chemical shift arguments, namely that, of the natural lysozyme variants that carry a mutation in the loop region of the β-domain, the mutant T70N tends to preserve the wild-type structure, in contrast to the D67H mutant that diverges significantly from the wild-type even before undergoing the pathologic amyloid transition.

Conformation of Relevant Side Chains—Because a drastic geometry change of a few side chains around the mutation site of D67H accompanies the loss of the wild-type H-bond network that has been considered to affect significantly the stability of the lysozyme β-domain (3), a detailed conformational analysis of some relevant side chains in variant T70N was attempted. Additional independent evidence was necessary to characterize in detail these structural features because of the resolution limits of the tethered MD results. In the wild-type structure, the side chain of residue 67 is involved in one or possibly two H-bonds to residue 70 (T70N-D67O$^{\delta1}$ and T70O$^{\gamma1}$-D67O$^{\delta1}$) (Fig. 6*a*). The number of H-bonds of residue 70 is conserved in the D67H mutant, although none of the original side chain H-bonds survives for the mutated residue (Fig. 6*b*). The examination of the NOESY and DQF-COSY pattern of T70N and wild-type lysozymes in H_2O and D_2O enabled us to conclude that both molecules possess the same conformation of the Asp-67 side chain with $\chi^1 \cong 60°$. This geometry is consistent with all coordinate sets available for the wild-type lysozyme from x-ray data and, because it can accommodate the mentioned H-bonds to residue 70, the question arises whether the mutation of threonyl into asparaginyl in T70N still supports those H-bonds. Unfortunately the spectra of the T70N lysozyme showed resonance degeneration for the two prochiral H^βs of Asn-70, which hinders extracting their diastereotopic assignments and the local conformation, as was done with Asp-67. The chemical equivalence of Asn-70 H^β resonances may be only fortuitous rather than due to rotational averaging that would not support an H-bond involvement of Asn-70 side-chain carboxyamide. High resolution one-dimensional NOESY measurements enabled us to measure precisely the chemical shifts of a few side-chain amides in the range 33–40 °C. The calculated chemical shift temperature coefficients of Asn-70 side-chain amides were −3 ppb/deg and −6 ppb/deg for the anti ($H^{\delta21}$) and syn ($H^{\delta22}$) amide resonances, respectively. Values between −6 and −8 ppb/deg were obtained also for other primary amide pairs of the T70N lysozyme. Because $|\Delta\delta/\Delta T| >$ 4–5 ppb/deg is typically observed for solvent-exposed primary and secondary amides when not involved in intramolecular H-bonds, our result is consistent with the occurrence of an H-bond at the Asn-70 anti-amide hydrogen. According to the structure obtained from the tethered MD calculation described previously, Asn-70 $H^{\delta21}$ could form two simultaneous H-bonds with Asp-67 and Ser-61 side-chain oxygen atoms, with the Asp-67 side chain adopting a χ^1 value close to 60 °. Thus two independent lines of evidence converge toward the same conclusion, namely that in the T70N lysozyme the spatial arrangement of the Asp-67 side chain is preserved along with some H-bonds that are part of the interaction network within the large loop of the β-domain in the wild-type lysozyme.

Isotope Exchange Measurements—To further confirm the previous structural conclusions, ^{1}H-^{2}H amide exchange rate determinations were performed on the mutant T70N. The protection factors were calculated from the experimental apparent kinetic constants. The values should be compared with the analogous data obtained for the wild-type and the mutant D67H (7), as shown in Fig. 7, for a specific selection. Apart from a few limited local discrepancies, which are likely to arise from the specific experimental conditions of each determination, the most important difference among our and previous data sets is observed in the segment 65–90, comprising the last stretch of the four-stranded sheet, the loop, the 3_{10} helix, and the connection turn to helix C (according to the wild-type protein geometry). In particular, in T70N the NH of Cys-65 recovers the extremely high protection factor that is lost in mutant D67H,

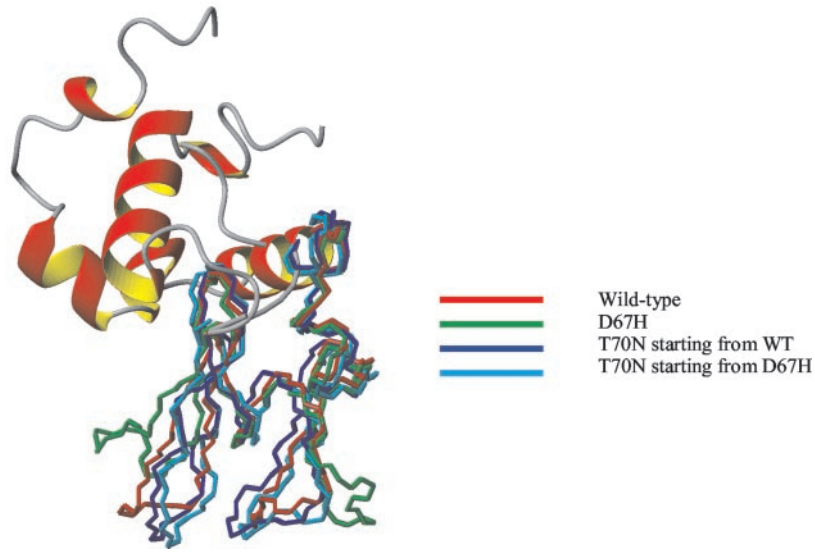

FIG. 5. **Best-fit superposition of the wild-type and D67H lysozyme crystal structures with the NMR-restrained tethered MD structures of the T70N variant.** The MD structures of the T70N lysozyme were obtained starting alternatively from the crystal structures of wild-type and D67H lysozymes (PDB codes 1REX and 1LYY, respectively). No other restriction, besides the experimental NMR distances, was imposed within the region 41–92. In the structure of wild-type human lysozyme, the selected fragment includes the residues of the β-sheet (four β-strands and intervening turns) and its interface with the α-domain (loop and 3_{10} helix segments). The best fit was calculated only outside the untethered region for all four structures, and a single ribbon trace was drawn for the tethered moiety. The C^{α} trace for fragment 41–92 of the four structures was drawn in different colors (*red*, wild-type; *green*, D67H; *blue*, T70N from wild-type; *cyan*, T70N from D67H).

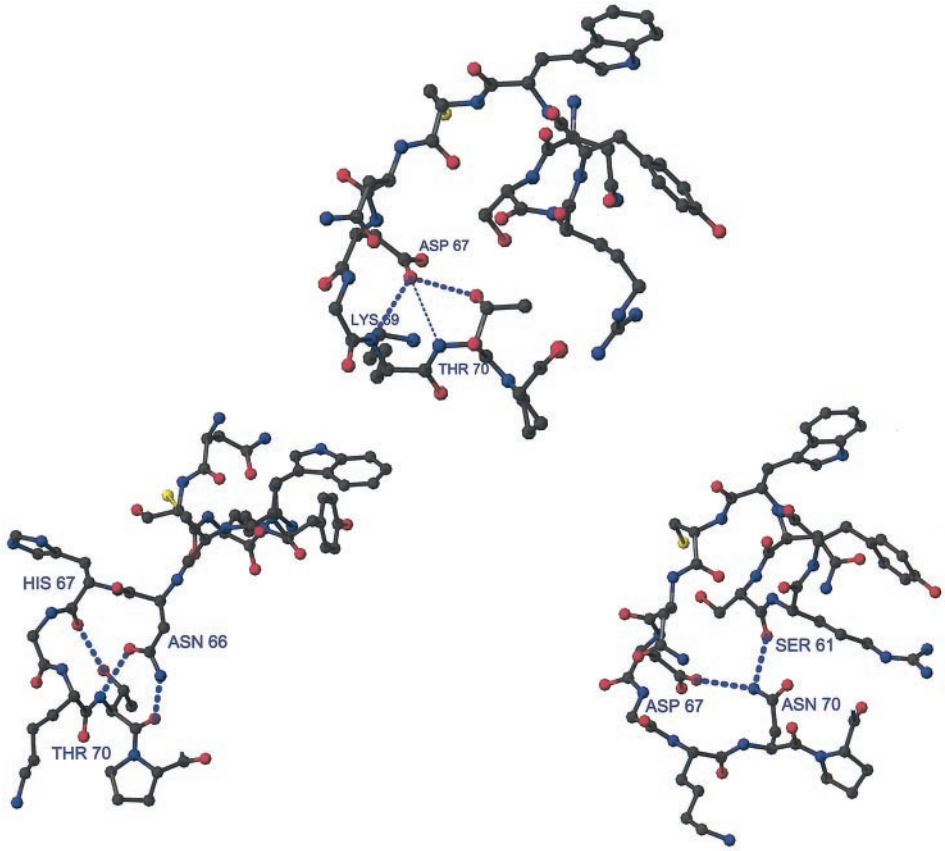

FIG. 6. **Conformation of relevant side chains.** H-bonding patterns within the β-domain large loop are shown as follows: wild-type, 69 N · · · 67 OD1 (0.437), 70 N · · · 67OD1 (0.175), 70 OG1 · · · 67 OD1 (0.661) (*a*); D67H, 66 ND2 · · · 70 O (0.59), 70 N · · · 66 OD1 (0.649), 70 OG1 · · · 67 O (0.503) (*b*); and the T70N lysozyme, 70 ND2 · · · 61 O (0.459), 70 ND2 · · · 67 OD1 (0.289), 73 N · · · 70 O (0.045) (*c*). The occurrence of hydrogen bonds was ascertained using the software WHATIF (38) with a routine that positions polar hydrogen atoms by optimizing the total hydrogen bond energy (26). A score between 0 and 1, reported in brackets, is given for each possible hydrogen bond and takes into account donor/acceptor types, the H-acceptor distance, the donor-H-acceptor angle, and the position of the H with respect to the acceptor. In all panels only the heavy atoms are shown, and the color code is as follows: *gray*, carbon; *blue*, nitrogen; *red*, oxygen; and *yellow*, sulfur.

whereas for residue 66 a protection factor $>10^4$ is obtained. The 3_{10} helix appears more protected in mutant T70N than even in the wild-type protein. Four residues in T70N (83, 84, 85, and 86) exhibit slow or moderately slow amide exchange, with protection factors ranging between 200 and 5000, against only two residues (84 and 85) in the wild-type protein. A similar degree of protection is observed also for the amides of residues 74, 77, 79, and 90 of T70N. The same amides, instead, were reported to exhibit no exchange protection in the D67H variant in the comparative study with the wild-type species (7). Previous qualitative ^1H-^2H exchange data on human lysozyme at pH 3.8 had shown slow amide exchange rates for residues 65, 66, 76, and 77 and intermediate rates for residues 79 and 86 (23). Therefore the amide exchange pattern of the T70N lysozyme can be considered quite related to that of the wild-type protein.

DISCUSSION

Linking Functional and Structural Properties of T70N Variant—Compared with the structure of wild-type lysozyme, the T70N replacement generates a more compact arrangement at the interface between the β-sheet and subsequent loop from one side and part of the α domain from the other side. In particular, the large loop 66–74 moves toward helix C, followed by β-sheet 42–55 that extends in a plane nearly perpendicular to the former loop and thus shifts away from helix D. This is the opposite of the conformational variation observed in mutant D67H (3). Based on the deuterium exchange results, some

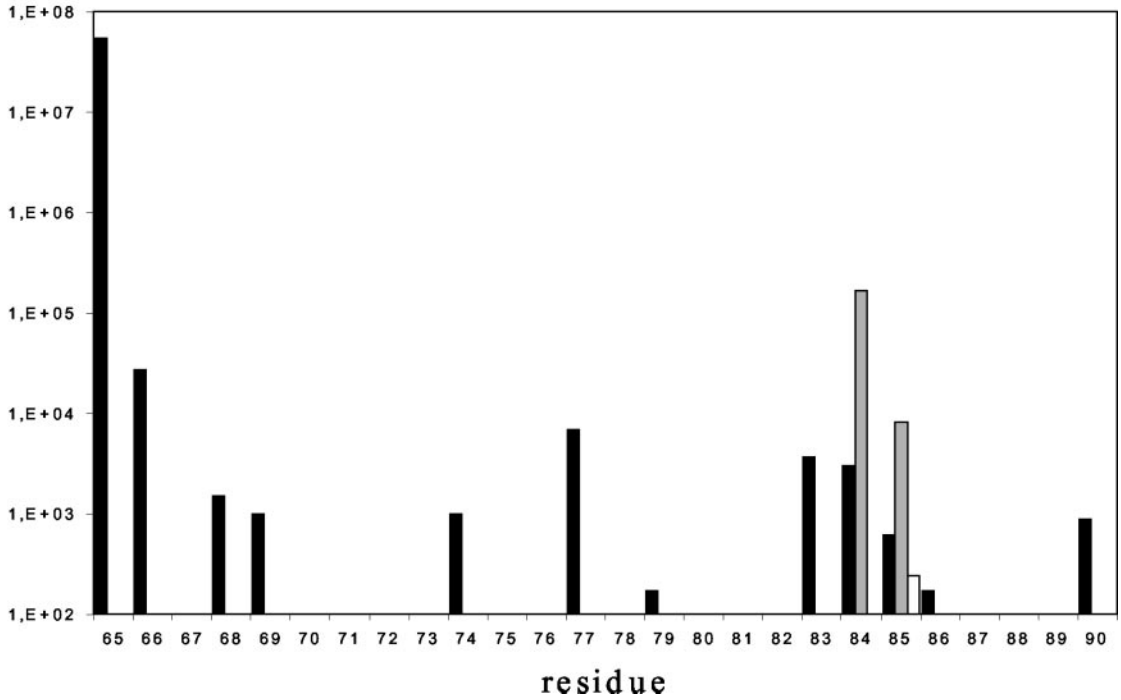

FIG. 7. **Comparison of the protection factors.** Protection factors within the fragment 65–90 of T70N (*black bars*), wild-type (*gray bars*), and D67H (*white bars*) lysozyme. The bar is not reported on the scale when the corresponding protection factor value was below 10^2. The values for wild-type and D67H are taken from Canet *et al.* (7).

additional structural deviations of T70N lysozyme should occur in regions further apart from the mutation site. The differences should concern the Ser-80 capping role, the actual extension of the 3_{10} helix, and the angle between the latter and helix C as imposed by the intervening turn. However, the extent of divergence of T70N from the wild-type structure is much more limited than the deviations observed with the D67H mutant, and, overall, when compared with the latter, T70N resembles the wild-type species much more closely (Fig. 5). The network of H-bonds that stabilizes the β-domain of lysozyme (3) appears preserved in the variant containing asparagine at position 70, as demonstrated by direct determination of conformation and H-bond involvement for the side chains of Asp-67 and Asn-70, respectively (Fig. 6). In the wild-type structure, that network connects Thr-52, Tyr-54, Ser-61, Asp-67, and Thr-70, and its rupture in the D67H mutant determines extensive structural modifications and pathological destabilization (3). Similar effects have been documented also for mutation at residue 70 with Ala and Val (29). The T70A substitution results in local disorder that prevents structure determination. The analogous mutation into Val, however, induces a significant rearrangement in the region 68–78 that preserves the local geometry and packing through the involvement of the Lys-69 side chain for the H-bonds and that of Arg-62 and Tyr-63 for interaction with the isopropyl group. Indeed, at 64.9 °C and pH 2.7, mutant T70V is destabilized by 2.9 kJ/mol with respect to wild-type, whereas T70A loses 6.2 kJ/mol of stability (29). The structural elements obtained by our ^{1}H NMR study qualitatively account for the stability properties of T70N. The wild-type packing geometry between the β and α-domains is largely preserved along with the H-bonding pattern within the β-domain loop. Thus, the corresponding contributions to the folding free energy should be conserved as well. Based on the analogy of the comparison between T70V and T70A or the T70N and D67H mutants, one may be tempted to link, in any lysozyme, the conservation of the H-bond network of the β-domain or the whole structure with folding stability. The significant destabilization of mutant I56T, despite substantial invariance with respect to wild-type fold (3), suggests that such a generalization may be too simplistic and risky. The features of the H-bond network of the β-domain should be explicitly addressed. In addition, the surface hydration structure should also be considered (30) before drawing stability conclusions from structural invariance.

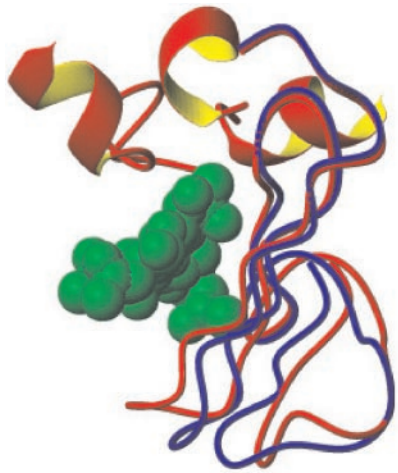

FIG. 8. **Best fit superposition of wild-type lysozyme-NAG complex (PDB ID 1LZR) and the T70N lysozyme in the region of the catalytic site.** The wild-type protein structures with and without substrate do not show any major difference in practice. A single ribbon trace is drawn outside the region 42–90. The C^{α} traces are *red* for wild-type and *blue* for the T70N variant. The presence of the substrate, shown as a *green* space-filling model, highlights the increased width of the catalytic cleft in the variant protein.

The ^{1}H NMR results qualitatively account for the activity loss of T70N also (Table I). Because of the shift of β-sheet 42–55, the width of the catalytic cleft is increased compared with that of the wild-type protein (Fig. 8), and, hence, a decrease of affinity should ensue that is expected to become more evident the smaller the substrates or inhibitors are. A decreased affinity should be responsible for the significant in-

crease of the equilibrium dissociation constant of T70N and the $(NAG)_3$ inhibitor. Along the same lines, one can also explain the data obtained with the chitin oligosaccharide used for testing the catalytic activities. The K_m of T70N increases and reaches a similar value to that seen for the pathologic mutant D67H, for which the activity loss results from a more complex conformational rearrangement. Overall however, the affinity loss is reduced with a substrate larger than the $(NAG)_3$ inhibitor as argued from comparison of K_m and K_d values (Table I).

The T70N Variant Is Less Destabilized Compared with the I56T and D67H Amyloidogenic Variants—The equilibrium unfolding experiments show that the T70N variant is less stable than the wild-type lysozyme. Nevertheless, the free energy destabilization resulting from mutation is less pronounced than that resulting from the previously characterized amyloidogenic variants I56T and D67H. This "intermediate" behavior of the T70N variant is also observed in its unfolding rate, which is faster than that of the wild-type but slower than those of the two amyloidogenic variants. Finally, as discussed above, the structural perturbation derived from the T70N substitution is not as marked as that resulting from the two established amyloidogenic mutations. These three observations are all correlated. The minor structural perturbation of the T70N variant, compared with those of the amyloidogenic variants, indeed results in a lower free energy destabilization and a less important acceleration of the unfolding reaction. The ultimate result is that the partially denatured state that is thought to promote fibrillogenesis of lysozyme *in vivo* (3, 7) is not as significantly populated as in patients in which one of the two amyloidogenic variants is present. Fully consistent with these data are the results obtained by monitoring thermodenaturation in the near and far UV CD. By this analysis, one of the main differences in the unfolding pathways of normal and pathological species was previously highlighted (3). Temperature-dependent unfolding of the amyloidogenic variant appeared to be not cooperative, and the partially unfolded state was highly populated near the midpoint of unfolding. T70N, to the contrary, presents a cooperative unfolding transition in which the loss of tertiary and secondary structures are concomitant. These data prompt us to exclude the presence of the partially unfolded structure at the midpoint of denaturation for this new variant, and, even if the melting point is lower, the mode of denaturation appears to be quite similar to that reported for the wild-type lysozyme.

Concluding Remarks—Globular protein stability has been inversely correlated with the propensity to form amyloid fibrils *in vitro* (31–33). The T70N lysozyme variant represents, in the category of amyloidogenic proteins of medical interest, the first globular protein in which the mutation destabilizes the molecule but does not cause, *in vivo*, the pathological conversion of the globular protein into amyloid fibrils. The comparison of the properties shared by wild-type and T70N, on one side, with those shared by I56T and D67H, on the other, allows one to highlight the abnormalities involved *in vivo* in the genesis of amyloid disease. The biochemical effects of the mutation make this new lysozyme variant less active, less stable, and less protected than the wild-type form against a denaturing environment, but, notwithstanding the destabilizing mutation, the level of amide exchange protection is not affected or is even increased, as for helix 3–10. This means that the local stability, which contributes to the overall folding free energy, is preserved, *i.e.* structures, with unfolded deviation beyond a certain level to allow competitive formation of the amyloid aggregate, are poorly represented within the statistical ensemble of the native folded state (34). Therefore the conformational modifications induced by the replacement of Thr in position 70 with Asn minimize fluctuations from the folded to a partially folded or an unfolded state, which appears to be one of the key pathogenic properties of amyloidogenic variants (7). Thus the hypothesis that amyloid transition involves those fluctuations is consistent with our observations on T70N, wherein such fluctuations should be much less extensive than in the pathological variants. In the field of new therapeutic strategies against conformational diseases (35) in which pathogenic point mutations of target proteins affect their stability, the discovery of destabilized variants devoid of pathological implication bears the relevance of a finely adjusted model. As a matter of fact, stabilization through synthetic ligands is becoming a promising approach against these diseases, and encouraging experimental results have been provided for the amyloidogenic variants of transthyretin (36) or, for a completely different type of disease, the oncogenic variants of the p53 protein (37). The demonstration of the existence of thermodynamic and kinetic thresholds that are lower than those of wild-type proteins but still adequate to protect from the pathological conversion suggests that conformational diseases could be prevented even with a partial stabilization of the pathological proteins.

Acknowledgments—We are grateful to Prof. Mark Pepys for continuous support and valuable discussion. We thank Dr. Christina Redfield for providing the NMR data of I56T and D67H mutants. G. E. thanks Dr. A. Makek for assistance.

REFERENCES

1. Sunde, M., Serpell, L. C., Bartlam, M., Fraser, P. E., Pepys, M. B., and Blake, C. C. F. (1997) *J. Mol. Biol.* **273,** 729–739
2. Dobson C. M. (1999) *Trends Biochem. Sci.* **24,** 329–332
3. Booth, D. R., Sunde, M., Bellotti, V., Robinson, C. V., Hutchinson, W. L., Fraser. P. E., Hawkins, P. N., Dobson, C. M., Radford, S. E., Blake, C. C. F., and Pepys, M. B. (1997) *Nature* **385,** 787–793
4. Chamberlain, A. K., Receveur, V., Spencer, A., Redfield, C., and Dobson, C. M. (2001) *Protein Sci.* **10,** 2525–2530
5. Canet, D., Sunde, M., Last, A. M., Miranker, A., Spencer, A., Robinson, C. V., and Dobson, C. M. (1999) *Biochemistry* **38,** 6419–6427
6. Takano, K., Funahashi, J., and Yutani, K. (2001) *Eur. J. Biochem.* **268,** 155–159
7. Canet, D., Last, A. M., Tito, P., Sunde, M., Spencer, A., Archer, D. B., Redfield, C., Robinson, C. V., and Dobson C. M. (2002) *Nat. Struct. Biol.* **9,** 308–314
8. Morozova-Roche, L. A., Zurdo, J., Spencer, A., Noppe, W., Receveur, V., Archer, D. B., Joniau, M., and Dobson, C. M. (2000) *J. Struct. Biol.* **130,** 339–351
9. Booth, D. R., Pepys, M. B., and Hawkins, P. N. (2000) *Hum. Mutat.* **16,** 180
10. Santoro, M. M., and Bolen, D. W. (1988) *Biochemistry* **27,** 8063–8068
11. Nanjo, F., Sakai, K., and Usui, T. (1988) *J. Biochem.* **104,** 255–258
12. Muraki, M., Harata, K., and Jigami, Y. (1992) *Biochemistry* **31,** 9212–9219
13. Braunschweiler, L., and Ernst, R. R. (1983) *J. Magn. Reson.* **53,** 521–528
14. Piantini, U., Sørensen, O. W., and Ernst, R. R. (1982) *J. Am. Chem. Soc.* **104,** 6800–6801
15. Jeener, J., Meier, B. H., Bachmann, P., and Ernst, R. R. (1979) *J. Chem. Phys.* **71,** 286–292
16. Hwang, T. L., and Shaka, A. J. (1995) *J. Magn. Reson.* **112,** 275–279
17. Marion, D., and Wüthrich, K. (1983) *Biochem. Biophys. Res. Commun.* **113,** 967–974
18. States, D. J., Haberkorn, R. A., and Ruben, D. J. (1982) *J. Magn. Reson.* **48,** 286–292
19. Keeler, J., Clowes, R. T., Davis, A. L., and Laue, E. D. (1994) *Methods Enzymol.* **239,** 145–207
20. Bax, A., and Davis, D. G. (1985) *J. Magn. Reson.* **65,** 355–360
21. Shaka, A. J., Lee, C. J., and Pines, A. (1988) *J. Magn. Reson.* **77,** 274–293
22. Bai, Y., Milne, J. S., Mayne, L., and Englander, S. W. (1993) *Proteins Struct. Funct. Genet.* **17,** 75–86
23. Redfield, C., and Dobson, C. M. (1990) *Biochemistry* **29,** 7201–7214
24. Dayringer, H. E., Tramontano, A., Sprang, S. R., and Fletterick, R. J. (1986) *J. Mol. Graph.* **6,** 82–87
25. Gillmore, J. D., Booth, D. R., Madhoo, S., Pepys, M. B., and Hawkins, P. N. (1999) *Nephrol. Dial. Transplant.* **14,** 2639–2644
26. Hooft, R. W. (1996) *Proteins* **26,** 363–376
27. Wüthrich, K. (1986) *NMR Spectroscopy of Proteins and Nucleic Acids*, John Wiley & Sons, Inc., New York
28. Wishart, D. S., and Sykes, B. D. (1994) *Methods Enzymol.* **239,** 363–392
29. Takano, K., Yamagata, Y., Funahashi, J., Hioki, Y., Kuramitsu, S., and Yutani, K. (1999) *Biochemistry*, **38,** 12698–12708
30. Funahashi, J., Takano, K., Yamagata, Y., and Yutani, K. (2002) *J. Biol. Chem.*, **277,** 21792–21800
31. Chiti, F., Taddei, N., Bucciantini, M., White, P., Ramponi, G., and Dobson,

C. M. (2000) *EMBO J.* **7,** 1441–1449
32. McCutchen, S. L., Lai, Z. H., Miroy, G. J., Kelly, J. W., and Colon, W. (1995) *Biochemistry* **34,** 13527–13536
33. Hurle, M. R., Helms, L. R., Li, L., Chan, W., and Wetzel, R. A. (1994) *Proc. Natl. Acad. Sci. U. S. A.* **91,** 5446–5450
34. Luque, I., Leavitt, S. A., and Freire, E. (2002) *Annu. Rev. Biophys. Biomol. Struct.* **31,** 235–256
35. Carrell, R. W., and Lomas, D. A. (2002) *N. Engl. J. Med.* **346,** 45–53
36. Peterson, S. A., Klabunde, T., Lashuel, H. A., Purkey, H., Sacchettini, J. C., and Kelly, J. W. (1998) *Proc. Natl. Acad. Sci. U. S. A.* **95,** 12956–12960
37. Bullock, A. N., and Fersht, A. R. (2001) *Nat. Rev. Cancer* **1,** 68–76
38. Vriend, G. (1990) *J. Mol. Graph.* **8,** 52–56

Structural and Folding Dynamic Properties of the T70N Variant of Human Lysozyme

Gennaro Esposito, Julian Garcia, Palma Mangione, Sofia Giorgetti, Alessandra Corazza, Paolo Viglino, Fabrizio Chiti, Alessia Andreola, Pascal Dumy, David Booth, Philip N. Hawkins and Vittorio Bellotti

J. Biol. Chem. 2003, 278:25910-25918.
doi: 10.1074/jbc.M211000200 originally published online April 22, 2003
